

Article

# Performance Analysis of ARIS-NOMA Systems under Cascade Rician Channels

Xuliang Liu <sup>1</sup> , Xinwei Yue <sup>2,3,\*</sup>, Zhiping Lu <sup>4,5</sup> and Tianwei Hou <sup>6</sup><sup>1</sup> Yellow River Conservancy Technical Institute, Kaifeng 475001, China; liuxuliang@yrcti.edu.cn<sup>2</sup> Key Laboratory of Information and Communication Systems, Ministry of Information Industry, Beijing Information Science and Technology University, Beijing 100101, China<sup>3</sup> Key Laboratory of Modern Measurement and Control Technology, Ministry of Education, Beijing Information Science and Technology University, Beijing 100101, China<sup>4</sup> School of Information and Communication Engineering, Beijing University of Posts and Telecommunications, Beijing 100876, China; luzp@cict.com<sup>5</sup> State Key Laboratory of Wireless Mobile Communications (CICT), Beijing 100191, China<sup>6</sup> School of Electronic and Information Engineering, Beijing Jiaotong University, Beijing 100044, China; twhou@bjtu.edu.cn

\* Correspondence: xinwei.yue@bistu.edu.cn

**Abstract:** Active reconfigurable intelligent surface (ARIS) has sparked more attention due to its capability to overcome the impact of double fading. This paper introduces using an ARIS to aid non-orthogonal multiple access (NOMA) communications over cascade Rician fading channels, where the direct links between the base station and users are seriously blocked. By applying ARIS, it can amplify the superposed signals to overcome the double pass loss effect caused by passive RIS. Both ARIS and NOMA can have synergistic impacts on sixth-generation communication systems. New approximated and asymptotic expressions in terms of outage probability and ergodic data rate of the  $k$ -th user are deduced for ARIS-NOMA systems. Based on asymptotic analytical results, we further calculate the diversity order and high signal-to-noise ratio slope of the  $k$ -th user. Finally, the system throughput of ARIS-NOMA is discussed in the delay-constrained transmission mode. Monte Carlo numerical results are performed to verify that: (1) the outage behaviors of ARIS-NOMA are better than that of ARIS-assisted orthogonal multiple access (OMA); (2) as the impact of thermal noise caused by ARIS becomes larger, the communication performance from the base station to ARIS, then to users, becomes worse; (3) the ARIS-NOMA systems have the ability to provide the improved ergodic data rate relative to ARIS-OMA.

**Keywords:** active reconfigurable intelligent surface; non-orthogonal multiple access; performance analysis; cascade Rician fading channels



**Citation:** Liu, X.; Yue, X.; Lu, Z.; Hou, T. Performance Analysis of ARIS-NOMA Systems under Cascade Rician Channels. *Symmetry* **2024**, *16*, 321. <https://doi.org/10.3390/sym16030321>

Academic Editor: Michel Planat

Received: 18 January 2024

Revised: 1 February 2024

Accepted: 9 February 2024

Published: 7 March 2024



**Copyright:** © 2024 by the authors. Licensee MDPI, Basel, Switzerland. This article is an open access article distributed under the terms and conditions of the Creative Commons Attribution (CC BY) license (<https://creativecommons.org/licenses/by/4.0/>).

## 1. Introduction

With the continuous development of new business needs, the study of sixth-generation (6G) communication wireless has received a lot of attention from both industry and academic circles. The reconfigurable intelligent surface (RIS) has been proposed as one of the physical layer technologies in 6G networks [1,2], which is capable of transforming the direction of incident electromagnetic waves to the desired users with controllable amplitudes. Composed of passive reconfigurable elements, the passive RIS (PRIS) has the features of low energy consumption and loss in terms of auxiliary wireless communications, which cannot enlarge the energy of the incident wave [3]. Different from PRIS, active RIS (ARIS) (It is worth pointing out that the abbreviation of ARIS is used to make the full-text expressions more concise in the following paragraph) amplifies the incident signals by configuring some active reflection elements [4]. It is capable of overcoming the influence of multiplicative fading caused by PRIS. This type of ARIS provides a new solution to enhance wireless signal coverage and reduce the size of the surface array [5].

An important feature of 6G networks is support for large-scale connectivity and multi-user access. Non-orthogonal multiple access (NOMA) has been viewed as the key component of next-generation multiple access, which allows users to multiplex in the same physical resource [6]. During the implementation of NOMA, the superposed coding and successive interference cancellation (SIC) schemes are employed at the base station (BS) and receivers. In [7], the user fairness and achievable rate were guaranteed for non-orthogonal users by taking the NOMA transmission. As a further development, the authors of [8] studied the impact of hardware impairments on NOMA systems, where the outage probability was derived in the closed form. By selecting the optimal power allocation factor [9], the performance of NOMA systems is superior to that of orthogonal multiple access (OMA) over composite fading channels. In [10], the NOMA-based scheduling mechanism was investigated to overcome the co-channel interference. The design of NOMA beamforming was proposed to achieve the trade-off between complexity and network performance [11]. To enhance spectral efficiency, the authors of [12] analyzed the bit error performance of NOMA based on spatial modulation. Additionally, the cluster-free based NOMA transmission was developed in [13], where the flexible SIC was employed to eliminate the interference.

### 1.1. Previous Works

(1) Studies on PRIS-NOMA Systems: Up to now, many theses have introduced the PRIS to aid NOMA communications for the purpose of improving system capacity and coverage [14–16]. PRIS and NOMA complement each other and have a symmetry impact on 6G wireless networks. More specifically, the authors of [14] designed the PRIS-assisted NOMA transmission scheme, in which the outage behaviors of users were evaluated with an on-off control. In [15], the transmit power at the base station (BS) was compared between PRIS-NOMA and PRIS-OMA through the design of PRIS phase shifting. It was unveiled in [16] that the outage probability of PRIS-NOMA is lower than that of traditional relaying schemes. Considering downlink transmission, the beamforming design of PRIS-NOMA was discussed with power budget constraints [17]. The various applications of PRIS to NOMA systems were surveyed in [18], where the centralized PRIS deployment can enlarge the difference among users. The sum rate of PRIS-NOMA was discussed by partitioning the PRIS zone [19], which simplifies the detection SIC program for strong users. From a harvest energy perspective, the authors of [20] investigated the ergodic capacity of two pairing users for PRIS-NOMA networks using wireless information power transfer. In [21], the system sum rate of uplink PRIS-NOMA was analyzed by taking into consideration the direct links. Furthermore, the authors of [22] designed the equalizers and phase shift of uplink PRIS-NOMA to alleviate the interference aroused by imperfect SIC. From the direction of safety applications, the authors in [23] evaluated the security behaviors of PRIS-NOMA by using the on-off control method. In addition, the system achievable rates of aerial PRIS-NOMA were formulated by optimizing both the power allocation and passive beam [24].

(2) Studies on ARIS Assisted Systems: Compared to PRIS, many researchers have focused attention on the application of active RIS (ARIS) into wireless communication [25–27]. The superiority of ARIS is that it can solve the double fading influence faced by PRIS, which can overcome the double path loss from the source to PRIS, and then to the destinations. To solve these staple limitations, the authors of [28] studied the capacity performance gain brought by ARIS. It demonstrated that the RIS can provide a larger sum rate relative to PRIS. The achievable rate of an ARIS-assisted downlink system was investigated in [29], which revealed that ARIS should be deployed closer to the desired users with decreasing amplification power. The double path loss caused by PRIS was converted into the additional form when ARIS was introduced to wireless systems. On the condition of the same power budget, ARIS has the advantage of system throughput in comparison to PRIS [30]. Furthermore, the authors of [31] surveyed the energy efficiency of ARIS sub/fully-connected structures and showed that the sub-connected structure can reduce

power consumption. In [32], the weighted capacity of ARIS-aided wireless powered systems was highlighted by designing adaptive beamforming. The authors of [33] developed the hybrid relay/ARIS architectures, where the power consumption results are presented in detail. On this basis, a new hybrid PRIS/ARIS architecture was proposed in [34] in the presence of restricting the amplification factors. To shed light on radar communication, the authors of [35] investigated the detection probability of an ARIS-assisted radar system.

(3) Studies on ARIS-NOMA Systems: Along with ARIS's successful strides, the focus on the application of ARIS to NOMA systems has been extensively growing in wireless communications. In [36], the sum throughput of uplink ARIS-NOMA was studied by dividing the maximization problems into several sub-problems. From the perspective of constrained energy, the authors of [37] analyzed the attainable rate of ARIS-NOMA and confirmed that it can achieve a larger rate in comparison to ARIS-OMA. With the help of the reinforcement learning method, the authors in [38] researched the communication probability of the ARIS-aided energy harvesting NOMA system. An active surface-assisted NOMA scheme was outlined in [39], where the sum achievable capacity was derived to satisfy user requirements. In addition, an ARIS was used to aid rate-splitting multiple access [40], which has the ability to strike a tradeoff between resource efficiency and computational complexity. Recently, the authors in [41] investigated the performance of ARIS-NOMA by taking into consideration hardware impairments.

### 1.2. Motivation and Contributions

Although the above research works have supplied an essential understanding of PRIS and ARIS-assisted wireless communications, the examinations of ARIS-aided NOMA systems are still in the early stages. ARIS has the ability to amplify the reflecting signals at the expense of additional power consumption (i.e., by integrating current-inverting converters or asymmetric current mirrors and so on), which can improve coverage for the obstructed/faded BS-user links. Introducing ARIS to aid NOMA communications is an effective way to enhance the system spectrum efficiency. Theoretically speaking, the ARIS-NOMA systems have the ability to expand the coverage of desired users and offer nimble ARIS deployment. The existing ARIS-NOMA works formulated the maximized sum data rate from the perspective of optimization. For example, in [36], the uplink sum data rates of ARIS-NOMA with multiple antennas were discussed by exploiting alternating optimization. The throughput maximization of ARIS-NOMA was formulated in [37] with the design of beamforming. However, there are still few treatises on investigating the communication probability from the viewpoint of performance analysis. Additionally, the general fading channels, i.e., Rician channels are more suitable for ARIS-aided communication scenarios. Sparked by these reasons, we study the system performance of ARIS-NOMA in terms of outage probability and ergodic data rate over cascade Rician fading channels. The impact of thermal noise caused by ARIS on system performance is taken into consideration. The technical contributions of this treatise are outlined as follows.

1. We consider the application of ARIS to NOMA systems, which can conquer the double fading caused by PRIS. We derive the approximated outage probability expressions of the  $k$ -th user for ARIS-NOMA systems over cascade Rician fading channels. According to the asymptotic analyses, we calculate the diversity order of the  $k$ -th user in the high signal-to-noise ratio (SNR) ranges. We discuss the system throughput of ARIS-NOMA in delay-constrained transmission mode. We also evaluate the outage performance of the ARIS-OMA systems.
2. We further deduce the exact ergodic data rate expression of the  $k$ -th user for ARIS-NOMA systems. The high SNR slopes of ergodic data rates are presented in the high SNR ranges. We observe that the ARIS-NOMA systems can acquire a larger ergodic data rate relative to ARIS-OMA systems. As the thermal noise decreases, the ARIS-NOMA systems can accomplish larger ergodic data rates.
3. We evaluate the system throughput of ARIS-NOMA in both delay-constrained/tolerant transmission modes. We observe that the number of ARIS elements has a deeper

influence on the communication throughput. With the increase in ARIS elements, the strengthened system throughput of ARIS-NOMA can be achieved. We also see that ARIS-NOMA is able to provide better system throughput than ARIS-OMA.

### 1.3. Organization and Notation

The remainder of this treatise is organized as follows. In Section 2, the system model of ARIS-assisted multiple users NOMA is introduced. The outage probability of multiple users for ARIS-NOMA is evaluated in Section 3. More specially, the approximate expressions of outage probability for user  $n$  and user  $m$  are provided. Section 4 provides the ergodic data rates of a pair of users. Computer simulation results are given in Section 5, and then Section 6 provides the conclusion. The proof processes are summed up in the Appendix A.

Notation: The main notations used in this treatise are listed as follows. The cumulative distribution function (CDF) and probability density function (PDF) of a random variable  $X$  are denoted by  $F_X(\cdot)$  and  $f_X(\cdot)$ , separately;  $\mathbb{E}\{\cdot\}$  and  $\mathbb{D}\{\cdot\}$  separately denote the expectation and variance operations; the superscript  $(\cdot)^H$  represents the conjugate-transpose operation.

## 2. System Model

As illustrated in Figure 1, we consider an ARIS-assisted downlink NOMA system, where the ARIS equipped with  $L$  reflecting elements is arranged to improve the cell coverage from the base station (BS) to  $K$  single-antenna users. The BS is equipped with a single antenna as well. Assume that the direct communication paths from BS to non-orthogonal users are obstructed or experience deep fading and communications with the help of ARIS. We assume that all wireless channels of ARIS-NOMA systems undergo large-scale and small-scale fading. The effective baseband channels from the BS to ARIS, and from ARIS to the  $k$ -th user are modeled as Rician fading channels, which are denoted as  $\mathbf{h}_{sr} \in \mathbb{C}^{L \times 1}$ ,  $\mathbf{h}_{rk} \in \mathbb{C}^{L \times 1}$ , separately. The channel coefficients  $\mathbf{h}_{sr} = \sqrt{d_{sr}^{-\alpha}} [h_{sr}^1, \dots, h_{sr}^L]^H$ ,  $\mathbf{h}_{rk} = \sqrt{d_{rk}^{-\alpha}} [h_{rk}^1, \dots, h_{rk}^L]^H$ , in which  $h_{rk}^l = \sqrt{\frac{\kappa}{\kappa+1}} + \sqrt{\frac{\kappa}{\kappa+1}} \tilde{h}_{rk}^l$  and  $\kappa$  denotes the Rician factor.  $d_{sr}$  and  $d_{rk}$  are the distances from BS to ARIS, and from ARIS to the  $k$ -th user, separately.  $\alpha$  is the path loss exponent.  $\tilde{h}_{sr}^l \sim \mathcal{CN}(0, 1)$  and  $\tilde{h}_{rk}^l \sim \mathcal{CN}(0, 1)$  are the complex channel coefficients from the BS and the  $l$ -th element of ARIS, and the  $l$ -th element of ARIS to the  $k$ -th user, respectively. The reflection diagonal matrix of ARIS is defined as  $\Theta = \text{diag}(\sqrt{\beta_1}e^{j\theta_1}, \dots, \sqrt{\beta_L}e^{j\theta_L})$ , where  $\beta_l$  is the amplitude coefficient of the  $l$ -th reflection element, and greater than *one* due to its amplification function.  $\theta_l$  denotes the phase shifting of the  $l$ -th reflection element, which can be used for the purpose of beamforming and signal alignment. Without loss of generality, the cascade baseband channels from the BS to ARIS, and then from ARIS to non-orthogonal users are ordered as  $|\mathbf{h}_{rK}^H \Theta \mathbf{h}_{sr}|^2 > \dots > |\mathbf{h}_{rk}^H \Theta \mathbf{h}_{sr}|^2 > |\mathbf{h}_{rj}^H \Theta \mathbf{h}_{sr}|^2 > \dots > |\mathbf{h}_{r1}^H \Theta \mathbf{h}_{sr}|^2$ . For clarity of predigestion, we assume that the far-field region is taken into account, where the transceiver distance is larger than the Rayleigh distance. The phase of the array steering vector can be linearly approximated for different elements, which makes mathematical analysis tractable. In addition, the channel status information of ARIS-NOMA systems can be acquired by designing the pilot signals [25,42,43]. This idealized assumption and more details regarding the design of pilot signals will be relaxed in future works.

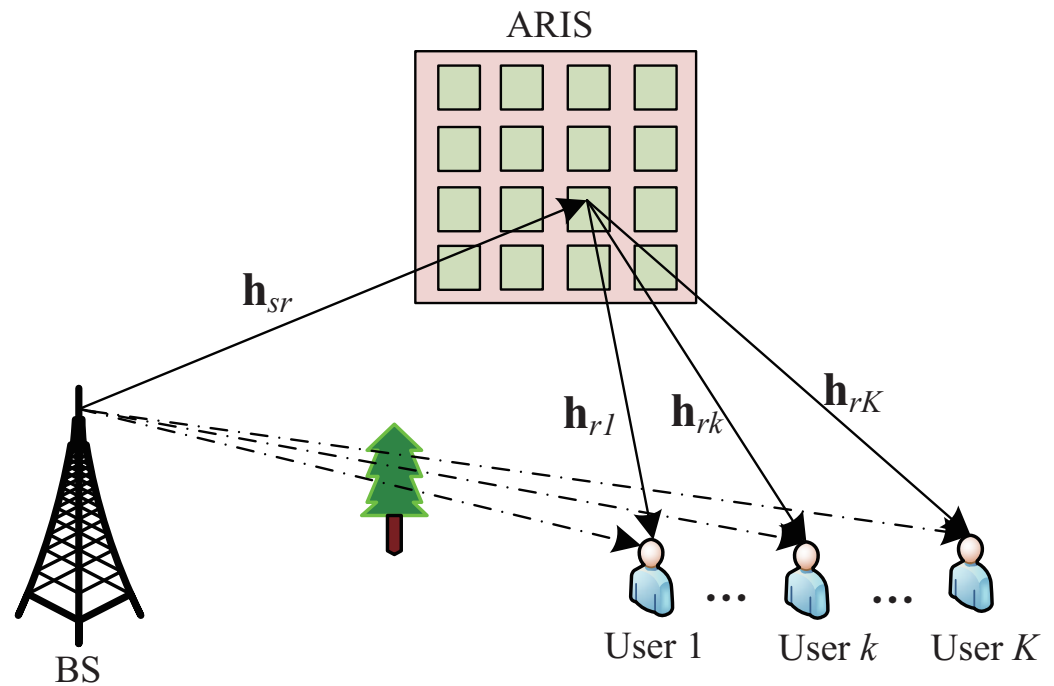


Figure 1. System model of ARIS-assisted NOMA communications..

### 2.1. Signal Expressions

For non-orthogonal transmission, the superimposed signals incoming to ARIS are amplified by active elements to destination nodes. At this moment, the received baseband signal at the  $k$ -user can be written as

$$y_k = \mathbf{h}_{rk}^H \mathbf{\Theta} \mathbf{h}_{sr} \sum_{i=1}^K \sqrt{a_i} P_s x_i + \mathbf{h}_{rk}^H \mathbf{\Theta} \mathbf{n}_r + n_k, \quad (1)$$

where  $x_i$  and  $a_i$  are the baseband signal and power allocation factor of the  $i$ -th user, which satisfy the conditions with  $\mathbb{E}\{x_i^2\} = 1$ . To guarantee users' fairness, the power allocation factors are satisfied; the following conditions, i.e.,  $a_1 > a_2 > \dots > a_k > \dots > a_K$  and  $\sum_{i=1}^K a_i = 1$ .  $P_s$  is the transmit power at BS.  $\mathbf{n}_r \sim \mathcal{CN}(0, N_r \mathbf{I}_L)$  denotes the thermal noise at ARIS with the noise power  $N_r$ , and  $\mathbf{I}_L \in \mathbb{C}^{L \times 1}$  is the identity matrix. Since the low-power amplifiers are pulled in the reflection elements, the thermal noise introduced by ARIS cannot be ignored smoothly.  $n_k \sim \mathcal{CN}(0, N_0)$  is the additive white Gaussian noise (AWGN) at the  $k$ -th user, which has zero mean and variance  $N_0$ .

Applying the SIC schemes, we assume that the  $k$ -th user can detect the front  $j - 1$  users' information successfully. Then the  $k$ -th user detects the  $j$ -th user's signal  $x_j$  and corresponding signal-to-interference-plus-noise ratio (SINR) can be written as

$$\gamma_{k \rightarrow j} = \frac{\beta |\mathbf{h}_{rk}^H \mathbf{\Lambda} \mathbf{h}_{sr}|^2 P_s a_j}{\beta |\mathbf{h}_{rk}^H \mathbf{\Lambda} \mathbf{h}_{sr}|^2 P_s \tilde{a}_j + \zeta \beta N_r |\mathbf{h}_{rk}^H \mathbf{\Lambda}|^2 + N_0}, \quad (2)$$

where  $\tilde{a}_j = \sum_{i=j+1}^K \sqrt{a_i}$ ,  $\mathbf{\Lambda} = \text{diag}(e^{j\theta_1}, \dots, e^{j\theta_l}, \dots, e^{j\theta_L})$  and  $\beta_l = \beta, \forall l \in L$ .  $\zeta$  represents the conversion factor. More specifically,  $\zeta = 1$  and  $\zeta = 0$  indicate the use of ARIS and PRIS to assist NOMA communications, respectively.

After cutting off the signal  $x_j$ , the SINR of  $k$ -th user decoding its own signal  $x_k$  can be given by

$$\gamma_k = \frac{\beta |\mathbf{h}_{rk}^H \mathbf{\Lambda} \mathbf{h}_{sr}|^2 P_s a_k}{\beta |\mathbf{h}_{rk}^H \mathbf{\Lambda} \mathbf{h}_{sr}|^2 P_s \tilde{a}_k + \zeta N_r \beta |\mathbf{h}_{rk}^H \mathbf{\Lambda}|^2 + N_0}. \quad (3)$$

Similar to the above detection process, the SINR at the  $K$ -th user to decode  $x_K$  can be given by

$$\gamma_K = \frac{\beta |\mathbf{h}_{rK}^H \mathbf{\Lambda} \mathbf{h}_{sr}|^2 P_s a_K}{\xi N_r \beta |\mathbf{h}_{rm}^H \mathbf{\Lambda}|^2 + N_0}. \quad (4)$$

## 2.2. ARIS-OMA Benchmark

The ARIS-OMA transmission mode is regarded as a benchmark for comparing the performance of ARIS-NOMA (Noting that other existing NOMA systems, such as sparse code multiple access (SCMA), pattern division multiple access (PDMA), interleaved division multiple access (IDMA), and rate splitting multiple access (RSMA), will be selected as the benchmarks in our future works) where the orthogonal signal is transmitted to a single orthogonal user, i.e.,  $U_o$  to avoid interference. In this communication scenario, detecting the SINR of  $U_o$  can be expressed as

$$\gamma_{U_o} = \frac{\beta |\mathbf{h}_{ro}^H \mathbf{\Lambda} \mathbf{h}_{sr}|^2 P_s}{\xi \beta N_r \|\mathbf{h}_{ro}^H \mathbf{\Lambda}\|^2 + N_0}, \quad (5)$$

where  $\mathbf{h}_{ro} = \sqrt{d_{ro}^{-\alpha}} [h_{ro}^1, \dots, h_{ro}^l, \dots, h_{ro}^L]^H$  represents the channel coefficient from an ARIS to  $U_o$ , and  $d_o$  denotes the distance from the ARIS to  $U_o$ .

## 3. Outage Probability

In this section, we make use of outage probability to evaluate the performance of ARIS-NOMA systems over cascade Rician channels. In this communication scenario, if the  $k$ -th user can not successfully detect the signal of any user in the previous  $k - 1$  users in front, the communication processes from the BS to ARIS and then to the  $k$ -th user will be interrupted. In other words, if the SINR of the  $k$ -th user detecting the  $j$ -th user's signal  $x_j$  is below the threshold of the target SNR, the outage occurs. In order to facilitate calculation, we can use the supplement event that the  $k$ -th user can detect the previous  $k - 1$  users' information [16,44]. Based on this interpretation, the outage probability of the  $k$ -th user for ARIS-NOMA systems can be expressed as

$$P_k = 1 - \Pr[\gamma_{k \rightarrow 1} > \gamma_{th1}, \dots, \gamma_{k \rightarrow j} > \gamma_{thj}, \gamma_k > \gamma_{thk}], \quad (6)$$

where  $\gamma_{thj} = 2^{R_{thj}} - 1$  denotes the target SNR with  $R_{thj}$  being the target data rate if the  $j$ -th user. The following theorem provides the theoretical analysis expression.

**Theorem 1.** The outage probability expression of the  $k$ -th user for ARIS-NOMA systems over cascade Rician channels can be approximated as

$$P_k \approx \Phi_K \sum_{t=0}^{K-k} \binom{K-k}{t} \frac{(-1)^t}{k+t} \left\{ \frac{\gamma(\delta_k + 1, \frac{\sqrt{\omega_k}}{\varepsilon_k})}{\Gamma(\delta_k + 1)} \right\}^{k+t}, \quad (7)$$

where  $\Phi_K = \frac{K!}{(K-k)!(k-1)!}$ ,  $\omega_k = \frac{\varphi_k}{\beta P_s} [\xi \beta N_r L \left( \frac{Lk+1}{k+1} \right) + N_0]$ ,  $\varphi_k = \max \left\{ \frac{\gamma_{th1}}{a_1 - \tilde{a}_1 \gamma_{th1}}, \dots, \frac{\gamma_{thj}}{a_j - \tilde{a}_j \gamma_{thj}}, \dots, \frac{\gamma_{thk}}{a_k - \tilde{a}_k \gamma_{thk}} \right\}$  and satisfying the conditions of  $a_1 > \tilde{a}_1 \gamma_{th1}, \dots, a_j > \tilde{a}_j \gamma_{thj}, \dots, a_k > \tilde{a}_k \gamma_{thk}$ .

$\delta_k = \frac{L \mathbb{E}(X_k)}{\mathbb{D}(X_k)}$ ,  $\varepsilon_k = \frac{\mathbb{D}(X_k)}{\mathbb{E}(X_k)}$ ,  $\mathbb{E}(X_k) = \mathbb{E}(|h_{sr}^l h_{rk}^l|) = \frac{\pi \sqrt{d_{sr}^{-\alpha} d_{rk}^{-\alpha}}}{4(\kappa+1)} [L_{\frac{1}{2}}(-\kappa)]^2$ ,  $\mathbb{D}(X_k) = d_{sr}^{-\alpha} d_{rk}^{-\alpha} \left\{ 1 - \frac{\pi^2}{16(\kappa+1)^2} [L_{\frac{1}{2}}(-\kappa)]^4 \right\}$ ,  $L_{\frac{1}{2}}(x) = e^{\frac{x}{2}} [(1-x)I_0(-\frac{x}{2}) - xI_1(-\frac{x}{2})]$  represents the Laguerre polynomial [45].  $I_0(\cdot)$  and  $I_1(\cdot)$  denote the modified Bessel functions of the first kind with orders zero and one, respectively, [46] [Equation (8.445)].  $\gamma(b, x) = \int_0^x t^{b-1} e^{-t} dt$  denotes the lower

incomplete Gamma function [46] [Equation (8.350.1)] and  $\Gamma(\cdot)$  denotes the gamma function [46] [Equation (8.310.1)].

**Proof.** See Appendix A.  $\square$

**Corollary 1.** For the special case of ARIS-NOMA systems, the outage probability expression of  $U_o$  for ARIS-OMA systems over cascade Rician channels is expressed as

$$P_{U_o} = [\Gamma(\delta_o + 1)]^{-1} \gamma\left(\delta_o + 1, \frac{\sqrt{\omega_o}}{\varepsilon_o}\right), \quad (8)$$

where  $\delta_o = \frac{L[\mathbb{E}(X_o)]^2}{\mathbb{D}(X_o)}$ ,  $\varepsilon_o = \frac{\mathbb{D}(X_o)}{\mathbb{E}(X_o)}$ ,  $\mathbb{E}(X_o) = \mathbb{E}\left(|h_{sr}^l h_{ro}^l|\right) = \frac{\pi\sqrt{d_{sr}^{-\alpha} d_{ro}^{-\alpha}}}{4(\kappa+1)} \left[L_{\frac{1}{2}}(-\kappa)\right]^2$ ,  $\mathbb{D}(X_o) = d_{sr}^{-\alpha} d_{ro}^{-\alpha} \left\{1 - \frac{\pi^2}{16(\kappa+1)^2} \left[L_{\frac{1}{2}}(-\kappa)\right]^4\right\}$ .  $\omega_o = \frac{\gamma_{tho}}{\beta P_s} \left[\xi \beta N_r L\left(\frac{L\kappa+1}{\kappa+1}\right) + N_0\right]$ ,  $\gamma_{tho} = 2^{R_{tho}} - 1$  denotes the target SNR of  $U_o$  with  $R_{tho}$  being the target data rate.

### 3.1. Diversity Analysis

In this subsection, we use the diversity order to evaluate the reliability of wireless communication links [47]. If the user can obtain the large diversity order, this indicates that the users' outage performance is quickly promoted in the high SNR ranges. On the contrary, they will be enhanced slowly. In particular, the diversity order of the  $k$ -th user for ARIS-NOMA systems can be calculated as

$$\hat{D} = - \lim_{\rho \rightarrow \infty} \frac{\log(P_k^\infty(\rho))}{\log \rho}, \quad (9)$$

where  $\rho = \frac{P_s}{N_0}$  denotes the transmitting SNR and  $P_k^\infty(\rho)$  denotes the asymptotic outage probability of the  $k$ -th user in the high SNR ranges.

**Corollary 2.** As  $P_s$  tends to  $\infty$ , the asymptotic outage probability expression of the  $k$ -th user for ARIS-NOMA systems is expressed as

$$P_k^\infty = \frac{K!}{(K-k)!k![(\delta_k+1)!]^k} \left(\frac{\sqrt{\omega}}{\varepsilon_n}\right)^{(\delta_k+1)k} \propto \frac{(\delta_k+1)k}{2}. \quad (10)$$

**Remark 1.** By substituting (10) into (9), the diversity order of the  $k$ -th user for ARIS-NOMA systems is equal to  $\frac{(\delta_k+1)k}{2}$ , which is related to the channel order, the number of reflecting elements, the Rician factor, and the distances from the BS to ARIS, and then to users.

**Corollary 3.** As  $P_s$  tends to  $\infty$ , the asymptotic outage probability expression of  $U_o$  for ARIS-OMA systems is expressed as

$$P_{U_o}^\infty = \frac{1}{\Gamma(\delta_o+1)(\delta_o+1)} \left(\frac{\sqrt{\omega_o}}{\varepsilon_o}\right)^{\delta_o+1} \propto \frac{\delta_o+1}{2}. \quad (11)$$

**Remark 2.** By substituting (11) into (9), the diversity order of  $U_o$  for ARIS-OMA systems is equal to  $\frac{\delta_o+1}{2}$ , which is only connected with the number of reflecting elements, Rician factor, and the distances from the BS to ARIS, and then to  $U_o$ .

### 3.2. Delay-Constrained Throughput

In the delay-constrained transmission mode, the system throughput of ARIS-NOMA depends on the effect of outage probability and target rate, which can be calculated as follows:

$$R_{ARIS}^{dl} = \sum_{k=1}^K (1 - P_k) R_{thk}, \quad (12)$$

where  $P_k$  can be obtained from (7) and  $R_{thk}$  denotes the  $k$ -th user's target rate.

#### 4. Ergodic Data Rate

In this section, we study the ergodic data rate performance over cascade Rician fading channels, which decides to maximize the transmission data rate of ARIS-NOMA systems. Assume that the  $k$ -th user can decode the information of the  $j$ -th user triumphantly. On the basis of (3), the ergodic data rate of  $k$ -th user can be expressed as

$$R_k^{erg} = \mathbb{E} \left[ \log \left( 1 + \frac{\beta |\mathbf{h}_{rk}^H \Lambda \mathbf{h}_{sr}|^2 P_s a_k}{\underbrace{\beta |\mathbf{h}_{rk}^H \Lambda \mathbf{h}_{sr}|^2 P_s \tilde{a}_k + \zeta \beta N_r |\mathbf{h}_{rk}^H \Lambda|^2 + N_0}_Z} \right) \right]. \quad (13)$$

As can be seen from the above equation, the closed-form expression of the ergodic data rate  $R_k^{erg}$  cannot be easily obtained. The following theorem provides the approximated expression.

**Theorem 2.** *The ergodic data rate expression of the  $k$ -th user for ARIS-NOMA systems over cascade Rician channels can be approximated as*

$$R_k^{erg} \approx \frac{a_k b_m}{\tilde{a}_k \ln 2} \left\{ \sum_{m=1}^M \frac{1}{1 + \psi} - \frac{\Phi_K}{1 + \psi} \sum_{t=0}^{K-k} \binom{K-k}{t} \frac{(-1)^t}{k+t} \right. \\ \left. \times \left( [\Gamma(\delta_k + 1)]^{-1} \gamma \left( \delta_k + 1, \frac{\sqrt{\hat{\omega}_k}}{\varepsilon_k} \right) \right)^{k+t} \right\}, \quad (14)$$

where  $b_k = \frac{\pi}{2M} \sqrt{1 - x_k^2}$ ,  $x_k = \cos\left(\frac{2k-1}{2M}\pi\right)$ ,  $\psi = \frac{(1+x_k)a_k}{2\tilde{a}_k}$  and  $\hat{\omega}_k = \frac{\psi}{(a_k - \tilde{a}_k\psi)\beta P_s} \times [\zeta \beta N_r L \left(\frac{Lk+1}{k+1}\right) + N_0]$  with the condition of  $a_k > \tilde{a}_k\psi$ .

**Proof.** The ergodic data rate expression in (13) can be further rewritten as

$$R_k^{erg} = \frac{1}{\ln 2} \int_0^\infty \frac{1 - F_Z(z)}{1+z} dz. \quad (15)$$

To acquire the expression of (14), we should firstly calculate the CDF of random variable  $Z$ . Applying order statistical characteristics and the specific solution can refer to the following processes:

$$F_Z(z) = \Pr \left( \frac{\beta |\mathbf{h}_{rk}^H \Lambda \mathbf{h}_{sr}|^2 P_s a_k}{\beta |\mathbf{h}_{rk}^H \Lambda \mathbf{h}_{sr}|^2 P_s \tilde{a}_k + \zeta N_r \beta |\mathbf{h}_{rk}^H \Lambda|^2 + N_0} < z \right) \\ = \Pr \left( |\mathbf{h}_{rk}^H \Lambda \mathbf{h}_{sr}|^2 < \frac{z(\zeta N_r \beta |\mathbf{h}_{rk}^H \Lambda|^2 + N_0)}{(a_k - z\tilde{a}_k)\beta P_s} \right) \\ = \Phi_K \sum_{t=0}^{K-k} \binom{K-k}{t} \frac{(-1)^t}{k+t} \left[ \frac{\gamma \left( \delta_k + 1, \frac{\sqrt{\hat{\omega}_k}}{\varepsilon_k} \right)}{\Gamma(\delta_k + 1)} \right]^{k+t}, \quad (16)$$

where  $z < \frac{a_k}{\bar{a}_k}$ . By substituting the above equation into (15), the ergodic data rate of the  $k$ -th user for ARIS-NOMA systems can be expressed as

$$R_k^{erg} = \frac{1}{\ln 2} \int_0^{\frac{a_k}{\bar{a}_k}} \frac{1}{1+z} dz - \frac{1}{\ln 2} \int_0^{\frac{a_k}{\bar{a}_k}} \frac{\Phi_K \sum_{t=0}^{K-k} \binom{K-k}{t} \frac{(-1)^t}{k+t} \left[ \frac{\gamma\left(\delta_k+1, \frac{\sqrt{\hat{\omega}_k}}{\varepsilon_k}\right)}{\Gamma(\delta_k+1)} \right]^{k+t}}{1+z} dz. \quad (17)$$

Applying the Gauss–Chebyshev method [45] into (17), we can obtain (14) and the proof is completed.  $\square$

**Corollary 4.** For the special case of ARIS-OMA systems, the ergodic data rate expression of  $U_o$  for ARIS-OMA systems over cascade Rician channels can be approximated as

$$R_{U_o}^{erg} = \frac{1}{\ln 2} \int_0^\infty \frac{1 - [\Gamma(\delta_o + 1)]^{-1} \gamma\left(\delta_o + 1, \frac{\sqrt{\hat{\omega}_o}}{\varepsilon_o}\right)}{1+x} dx. \quad (18)$$

#### 4.1. High SNR Slope Analysis

The high SNR slope analysis is usually selected as the metric to evaluate the performance of the ergodic data rate, which can depict how fast the ergodic data rate increases in the high SNR range. Hence, the high SNR slope of the ergodic data rate for the  $k$ -th user can be expressed as

$$\hat{S} = - \lim_{\rho \rightarrow \infty} \frac{R_{k,\infty}^{erg}(\rho)}{\log(\rho)}, \quad (19)$$

where  $R_{k,\infty}^{erg}(\rho)$  is the asymptotic ergodic data rate in the high SNR range.

According to (14), when  $P_s$  tends to  $\infty$ ,  $\hat{\omega}_k \rightarrow 0$ , the lower incomplete Gamma function can be approximated as

$$\gamma\left(\delta_k + 1, \frac{\sqrt{\hat{\omega}_k}}{\varepsilon_k}\right) \approx \frac{(\sqrt{\hat{\omega}_k})^{\delta_k+1}}{\delta_k + 1}. \quad (20)$$

Hence, the following corollary can provide the asymptotic ergodic data rate.

**Corollary 5.** By substituting (20) into (14), the asymptotic ergodic data rate of the  $k$ -th user for ARIS-NOMA systems can be given by

$$R_{k,\infty}^{erg} \approx \frac{a_k b_m}{\bar{a}_k \ln 2} \left\{ \sum_{m=1}^M \frac{1}{1+\psi} - \frac{\Phi_K}{1+\psi} \sum_{t=0}^{K-k} \binom{K-k}{t} \frac{(-1)^t}{k+t} \times \left( \frac{\hat{\omega}_k^{\frac{\delta_k+1}{2}}}{(\delta_k+1)\Gamma(\delta_k+1)} \right)^{k+t} \right\}. \quad (21)$$

**Remark 3.** By substituting (21) into (19), the high SNR slope of the  $k$ -th user is equivalent to zero. This is because the ergodic data rate of the  $k$ -th user has been affected by the thermal noise caused at ARIS.

**Corollary 6.** Similar to the solution processes of (21), when  $P_s$  tends to  $\infty$ , the asymptotic ergodic data rate of the  $k$ -th user for ARIS-NOMA systems can be given by

$$R_{U_0, \infty}^{erg} = \frac{1}{\ln 2} \int_0^\infty \frac{1 - [(\delta_0 + 1)\Gamma(\delta_0 + 1)]^{-1} \omega_0^{\frac{\delta_k + 1}{2}}}{1 + x} dx. \quad (22)$$

**Remark 4.** By substituting it into (19), the high SNR slope of  $U_0$  is also equivalent to one. As can be seen, the slope of the ergodic data rate is also affected by thermal noise.

#### 4.2. Delay-Tolerated Throughput

In the delay-tolerated transmission mode, the system throughput of ARIS-NOMA only depends on the ergodic data rate, which can be calculated as follows:

$$R_{ARIS}^{dtt} = \sum_{k=1}^K R_k^{erg}, \quad (23)$$

where  $R_k^{erg}$  can be obtained from (14).

### 5. Numerical Results

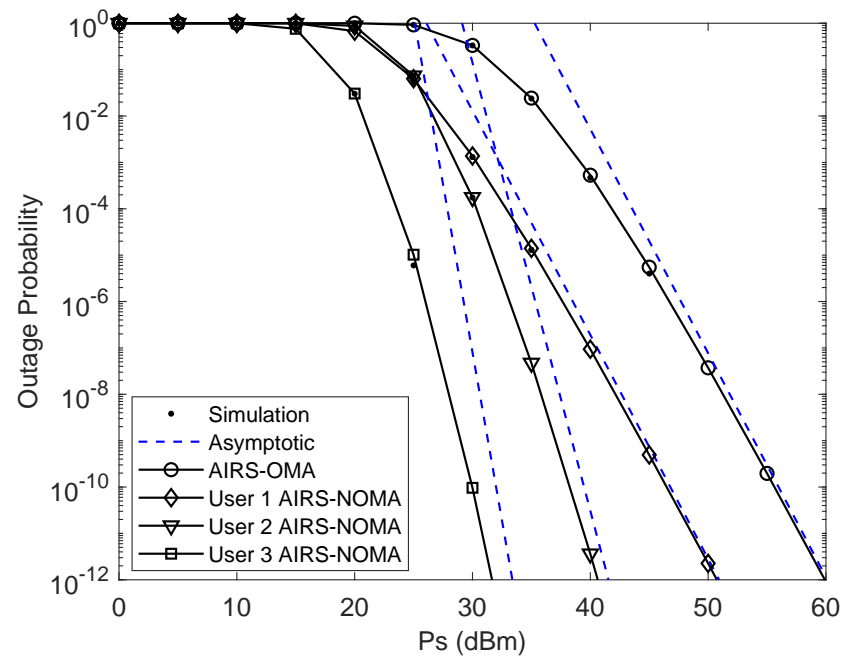
In this section, computer numerical results are provided to confirm the correctness of theoretical results derived in previous sections and evaluate the symmetry impact of thermal noise and other parameters on ARIS-NOMA. Unless there is a special statement, we set that there are three users, i.e.,  $K = 3$  in the system. The computer simulation parameters are listed as: the power allocation factors of users are set to  $a_1 = 0.7$ ,  $a_2 = 0.2$ , and  $a_3 = 0.1$ , separately. We also set the distances of  $d_{r1} = 20$  m,  $d_{r2} = 15$  m,  $d_{r3} = 10$  m, and  $d_{sr} = 15$  m. The thermal noise and AWGN powers are set to be  $N_r = N_0 = -30$  dBm [30]. The target data rates of users are set to be  $R_1 = R_2 = R_3 = 1$  bps/Hz. The number of reflection elements and amplitude coefficient of ARIS are separately set to be 6 and 3, respectively. In addition, the performance of ARIS-OMA systems is chosen as the baseline to compare with that of ARIS-NOMA systems.

#### 5.1. Outage Probability

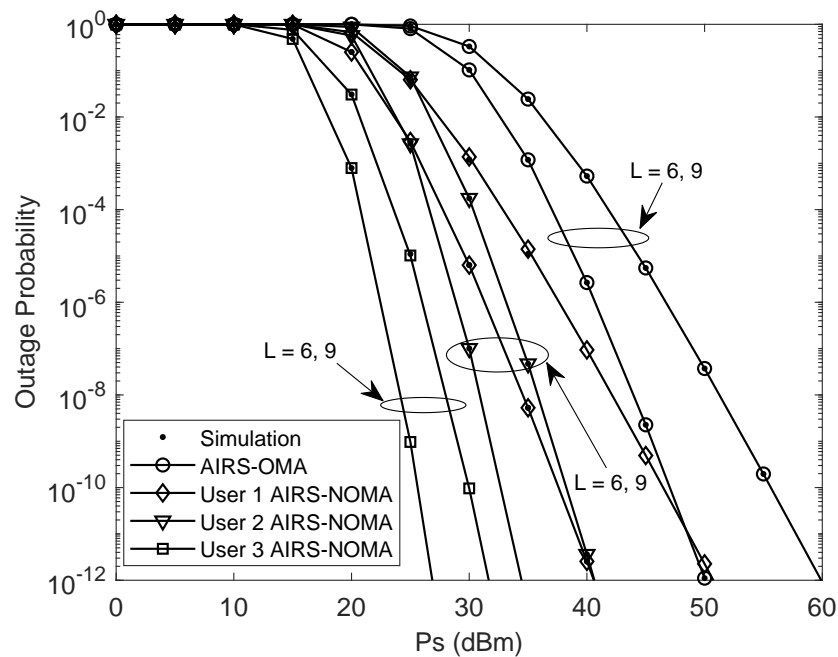
Figure 2 plots the outage probability of three non-orthogonal users versus  $P_s$ , with  $K = 3$ ,  $L = 6$ ,  $\beta = 3$ ,  $\alpha = 2$ , and  $R_1 = R_2 = R_3 = 1$  bps/Hz. The exact curves of outage probability for non-orthogonal users and  $U_0$  are plotted based on (7) and (10), respectively. It should be seen that the simulation results and theoretical analyses of ARIS-NOMA and ARIS-OMA almost coincide together. The asymptotic curves of outage probability for non-orthogonal users and  $U_0$  are plotted according to (10) and (11), separately. We can observe that the asymptotic outage behaviors converge to theoretical values in the high SNR ranges. We unveil that the outage behaviors of ARIS-NOMA are superior to that of ARIS-OMA. This is due to the fact that NOMA is able to provide more symmetry and communication fairness relative to OMA. Additionally, the application of ARIS into NOMA systems effectively solves the double fading caused by passive RIS and expands the cell coverage.

Figure 3 plots the outage probability of three non-orthogonal users versus  $P_s$  for a simulation with the different reflecting elements, where  $\beta = 3$ ,  $\kappa = -20$  dB,  $\alpha = 2$ ,  $K = 3$ ,  $N_r = N_0 = -30$  dBm, and  $R_1 = R_2 = R_3 = 1$  bps/Hz. As can be observed, with increasing the number of reflecting elements, the outage performance of ARIS-NOMA/OMA systems becomes much better, which is in line with the conclusions in the above parts. Hence, we can adjust the configuration of ARIS to adapt to the changing scenarios. The influence of thermal noise from ARIS is further illustrated by Figure 4, where  $\beta = 5$ ,  $\kappa = -20$  dB,  $\alpha = 2$ ,  $K = 3$ ,  $L = 6$ , and  $R_1 = R_2 = R_3 = 1$  bps/Hz. As the thermal noise power increases, the asymptotic performance gap decreases. There are no error floors in the figure, although the

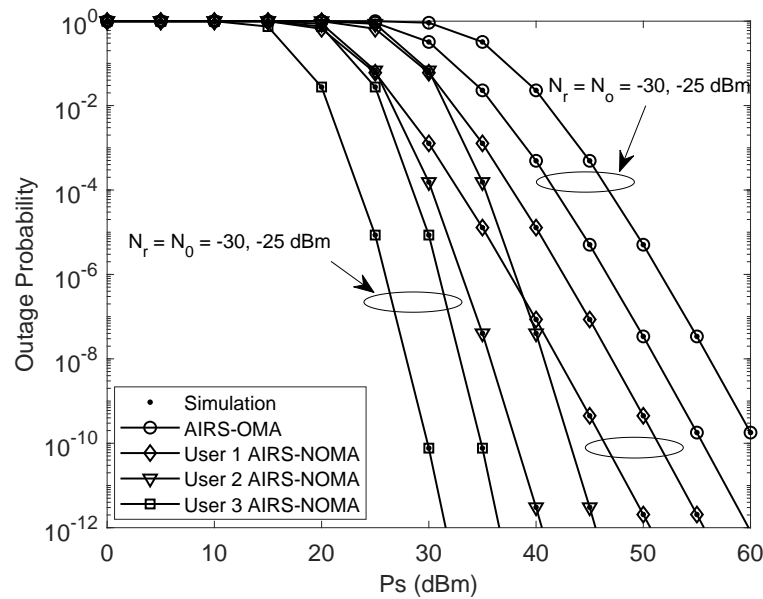
outage probability of ARIS-NOMA/OMA suffers from the thermal noise. This is due to the actual result that the thermal noise is modeled as the constant in the derived processes.



**Figure 2.** Outage probability versus  $P_s$ , with  $\beta = 3$ ,  $\kappa = -20$  dB,  $\alpha = 2$ ,  $K = 3$ ,  $L = 6$ ,  $N_r = N_0 = -30$  dBm, and  $R_1 = R_2 = R_3 = 1$  bps/Hz.

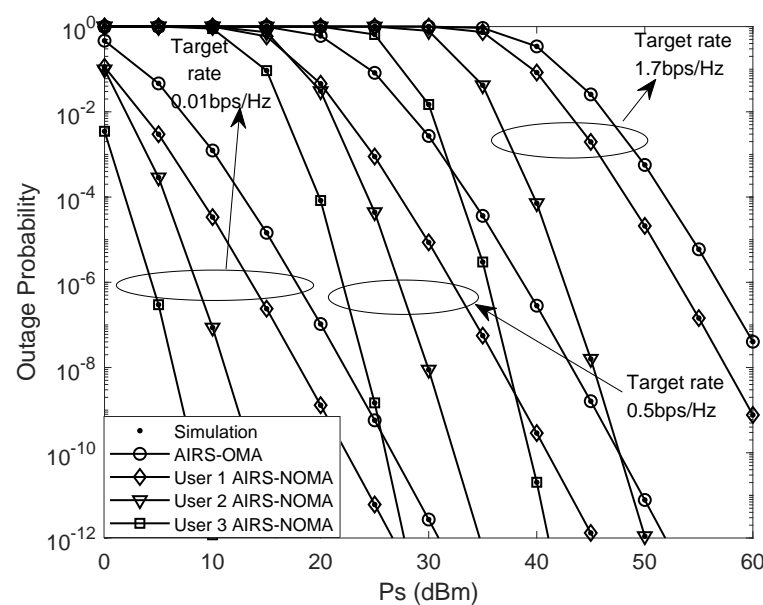


**Figure 3.** Outage probability versus  $P_s$ , with  $\beta = 3$ ,  $\kappa = -20$  dB,  $\alpha = 2$ ,  $K = 3$ ,  $N_r = N_0 = -30$  dBm, and  $R_1 = R_2 = R_3 = 1$  bps/Hz.

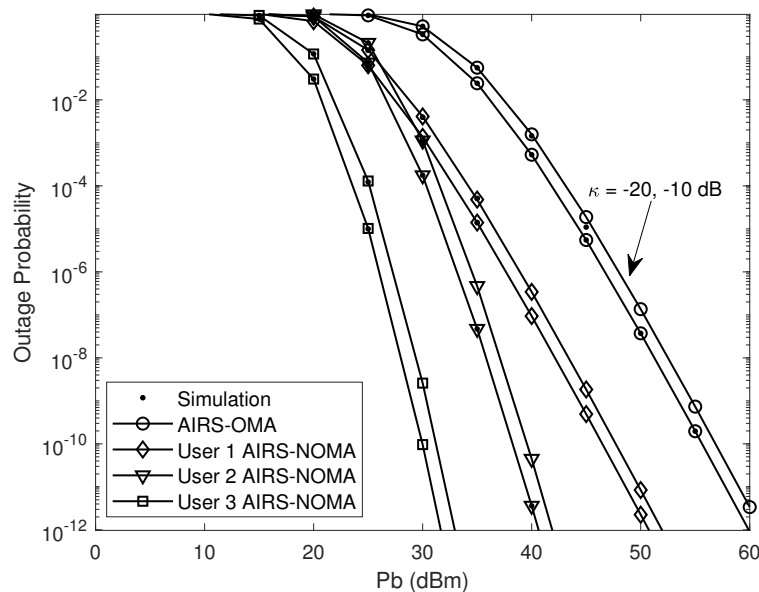


**Figure 4.** Outage probability versus  $P_s$ , with  $\beta = 5$ ,  $\kappa = -20$  dB,  $\alpha = 2$ ,  $K = 3$ ,  $L = 6$ , and  $R_1 = R_2 = R_3 = 1$  bps/Hz.

Figure 5 plots the outage probability of three non-orthogonal users versus  $P_s$  with different target data rates, where  $\beta = 5$ ,  $\kappa = -20$  dB,  $\alpha = 2$ ,  $K = 3$ ,  $L = 6$ , and  $N_r = N_0 = -30$  dBm. As can be seen from the figure, the outage probability of ARIS-NOMA is seriously affected by target data rates, while the setting of the smaller target data rates brings robust performance. This phenomenon denotes that the smaller target data rates can adapt to the requirements of Internet of Things scenarios. As a further advance, Figure 6 plots the impact of the Rician factor, i.e.,  $\kappa$  on outage behaviors of ARIS-NOMA/OMA systems. One can observe that with the increasing Rician factor, the performance of ARIS-NOMA/OMA becomes much better. The main reason is that the component of the line of sight (LoS) changes into the leading factor. In the RIS-assisted communication scenarios, more LoS paths can provide efficacious ways to strengthen the service quality for users.



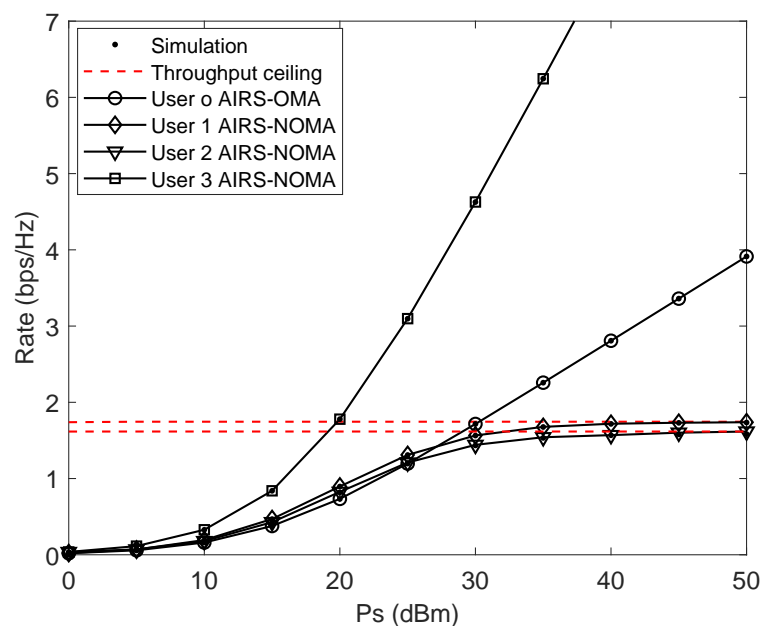
**Figure 5.** Outage probability versus  $P_s$ , with  $\beta = 5$ ,  $\kappa = -20$  dB,  $\alpha = 2$ ,  $K = 3$ ,  $L = 6$ , and  $N_r = N_0 = -30$  dBm.



**Figure 6.** Outage probability versus  $P_s$ , with  $\beta = 5$ ,  $\alpha = 2$ ,  $K = 3$ ,  $L = 6$ , and  $N_r = N_0 = -30$  dBm.

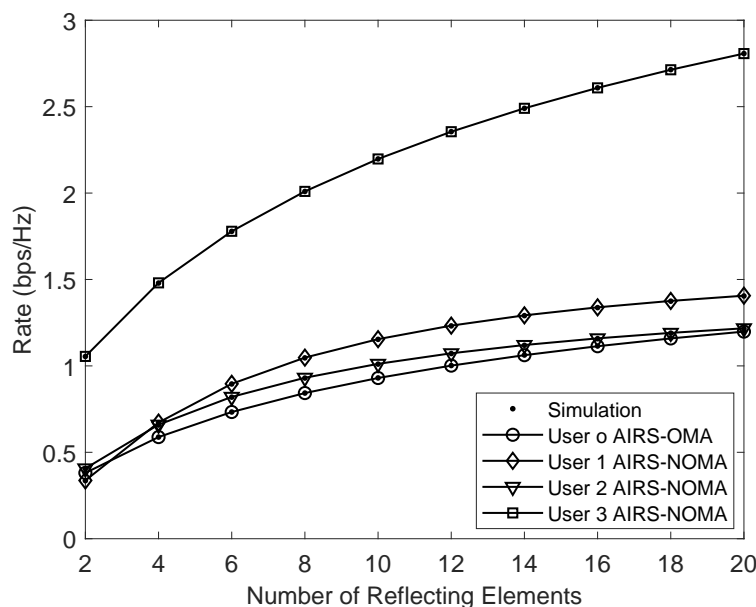
### 5.2. Ergodic Data Rate

Figure 7 plots ergodic data rates of three non-orthogonal users versus  $P_s$ , with  $\beta = 5$ ,  $\kappa = -20$  dB,  $\alpha = 2$ ,  $K = 3$ ,  $L = 6$ , and  $N_r = N_0 = -30$  dBm. The exact and asymptotic curves of ergodic data rate for ARIS-NOMA are plotted based on (14) and (21), respectively. The exact curves of the ergodic data rate for ARIS-NOMA and ARIS-OMA are plotted based on (10) and (22), respectively. The asymptotic curves coincide with the exact curve at high transmitting powers. We can observe from the figure that the ergodic data rate of the nearest non-orthogonal user outperforms that of the orthogonal user, while the ergodic data rates of the distant non-orthogonal users are inferior to that of the orthogonal user. The main reason is that ARIS-NOMA is capable of providing much more fairness compared to ARIS-OMA on the condition of multiple users.



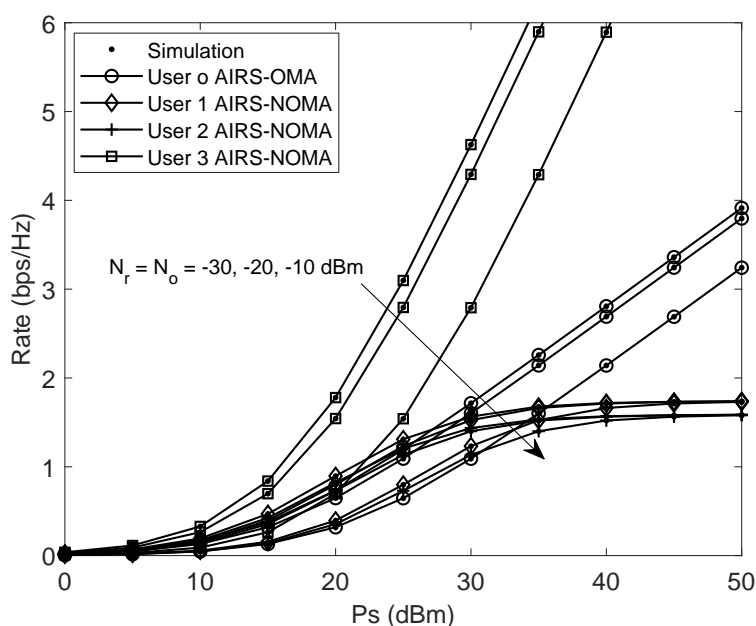
**Figure 7.** Ergodic data rate versus  $P_s$ , with  $\beta = 5$ ,  $\kappa = -20$  dB,  $\alpha = 2$ ,  $K = 3$ ,  $L = 6$ , and  $N_r = N_0 = -30$  dBm.

Figure 8 plots ergodic data rates of three non-orthogonal users versus the number of reflecting elements, with  $\beta = 5$ ,  $\kappa = -20$  dB,  $\alpha = 2$ ,  $K = 3$ , and  $N_r = N_0 = -30$  dBm. It is worth noting that by increasing the number of reflecting elements, the ergodic performance of the users becomes much better. This is because more reflecting elements can achieve the power enhancement of receiving signals for the users. Certainly, we also can increase the value of the amplification factor at each reflecting element to signal power enhancement.



**Figure 8.** Ergodic data rate versus  $P_s$ , with  $\beta = 5$ ,  $\kappa = -20$  dB,  $\alpha = 2$ ,  $K = 3$ , and  $N_r = N_0 = -30$  dBm.

Figure 9 plots the ergodic data rates of three non-orthogonal users versus  $P_s$  with different thermal noise power, where  $\beta = 5$ ,  $\kappa = -20$  dB,  $\alpha = 2$ , and  $K = 3$ . It is observed that as the thermal noise power decreases, the ergodic performance of the users is greatly subjoined. Hence, it is reasonable to reduce the thermal noise power caused by ARIS under the same amplification factors at reflecting elements.



**Figure 9.** Ergodic data rate versus  $P_s$ , with  $\beta = 5$ ,  $\kappa = -20$  dB,  $\alpha = 2$ , and  $K = 3$ .

### 5.3. System Throughput

Finally, Figures 10 and 11 plot the system throughput versus  $P_s$  in both delay-constrained and delay-tolerated transmission modes. As can be observed, the sum delay-constrained throughput of ARIS-NOMA and ARIS-OMA increases with  $L$ , since multiple reflecting elements bring the enhanced ARIS beamforming gains. In addition, the impact of thermal noise power on sum delay-tolerated throughput is presented for ARIS-NOMA and ARIS-OMA. We observe that as the thermal noise power increases, the sum of delay-tolerated throughput becomes smaller. Hence, it is important to cut down thermal noise power in an effective way.

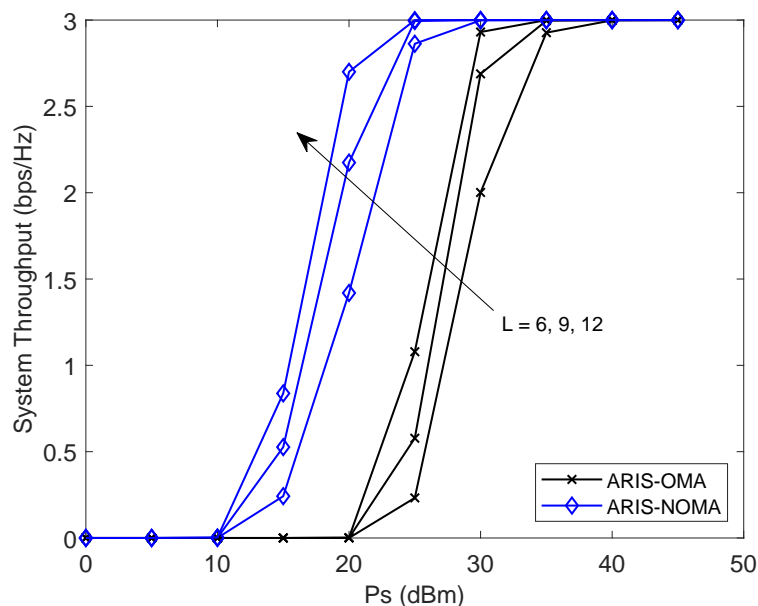


**Figure 10.** Delay-constrained system throughput versus  $P_s$ , with  $\beta = 5$ ,  $\kappa = -20$  dB,  $\alpha = 2$ , and  $K = 3$ .

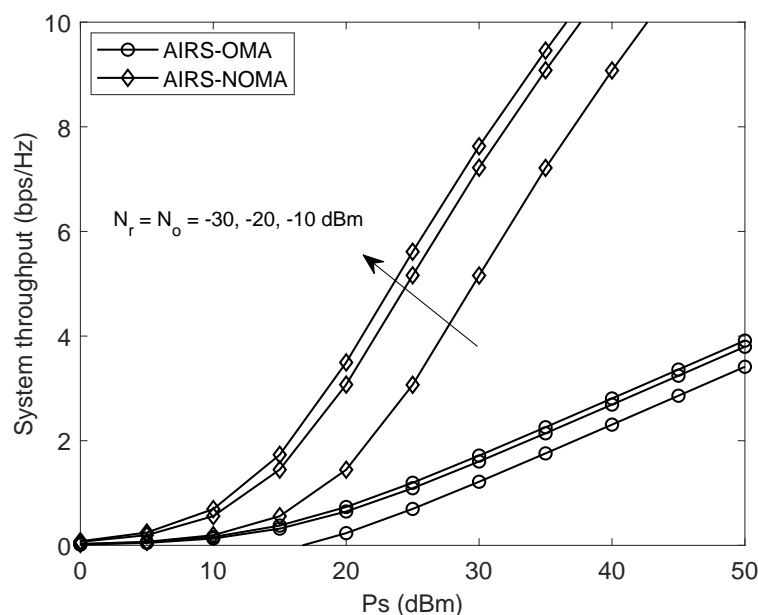


**Figure 11.** Delay-tolerated system throughput versus  $P_s$ , with  $\beta = 5$ ,  $\kappa = -20$  dB,  $\alpha = 2$ , and  $K = 3$ .

## 6. Conclusions

In this paper, we have researched the performance of ARIS-NOMA systems. Regarding cascade Rician fading channels, we surveyed the symmetry influence of the thermal noise

aroused by ARIS on NOMA systems. In particular, the exact outage probability and ergodic data rate expression were deduced. To gain deep insights, we presented the diversity orders and high SNR slopes of non-orthogonal users. The system throughput of ARIS-NOMA outperformed that of ARIS/PRIS-OMA systems in delay-constrained/tolerated transmit modes. Computer simulation results showed that the outage probability of ARIS-NOMA outshined that of ARIS/PRIS-OMA. The ergodic data rate of the nearest non-orthogonal user for ARIS-NOMA was larger than that of ARIS/PRIS-OMA.

**Author Contributions:** Conceptualization, X.L. and X.Y.; methodology, X.L. and X.Y.; validation, X.L. and X.Y.; formal analysis, X.L., X.Y., Z.L. and T.H.; investigation, X.L. and X.Y.; resources, X.L. and X.Y.; writing—original draft preparation, X.L. and X.Y.; writing—review and editing, X.L., X.Y., Z.L. and T.H.; supervision, Z.L. and T.H.; project administration, X.Y. and T.H. All authors have read and agreed to the published version of the manuscript.

**Funding:** This research was funded by Henan Province Science and Technology Research Project: Grant 232102320004.

**Data Availability Statement:** Data are contained within the article.

**Conflicts of Interest:** The authors declare no conflicts of interest.

## Appendix A

**Proof of Theorem 1.** Upon substituting (2) and (3) into (7), the outage probability expression of the  $k$ -th user for ARIS-NOMA systems can be written as

$$P_k = 1 - \Pr \left[ \frac{\beta |\mathbf{h}_{rk}^H \Lambda \mathbf{h}_{sr}|^2 P_s a_1}{\beta |\mathbf{h}_{rk}^H \Lambda \mathbf{h}_{sr}|^2 P_s \tilde{a}_1 + \zeta \beta N_r |\mathbf{h}_{rk}^H \Lambda|^2 + N_0} > \gamma_{th1}, \dots, \frac{\beta |\mathbf{h}_{rk}^H \Lambda \mathbf{h}_{sr}|^2 P_s a_j}{\beta |\mathbf{h}_{rk}^H \Lambda \mathbf{h}_{sr}|^2 P_s \tilde{a}_j + \zeta \beta N_r |\mathbf{h}_{rk}^H \Lambda|^2 + N_0} > \gamma_{thj}, \dots, \frac{\beta |\mathbf{h}_{rk}^H \Lambda \mathbf{h}_{sr}|^2 P_s a_k}{\beta |\mathbf{h}_{rk}^H \Lambda \mathbf{h}_{sr}|^2 P_s \tilde{a}_k + \zeta \beta N_r |\mathbf{h}_{rk}^H \Lambda|^2 + 1} > \gamma_{thk} \right]. \quad (\text{A1})$$

Applying some simple operations of the upper formula, the expression  $P_k$  can be rewritten as

$$P_k = \Pr \left\{ \underbrace{|\mathbf{h}_{rk}^H \Lambda \mathbf{h}_{sr}|^2}_X < \frac{\varphi_k}{\beta P_s} \left( \underbrace{\zeta \beta N_r |\mathbf{h}_{rk}^H \Lambda|^2 + N_0}_Y \right) \right\}, \quad (\text{A2})$$

where  $\varphi_k = \max \left\{ \frac{\gamma_{th1}}{a_1 - \tilde{a}_1 \gamma_{th1}}, \dots, \frac{\gamma_{thj}}{a_j - \tilde{a}_j \gamma_{thj}}, \dots, \frac{\gamma_{thk}}{a_k - \tilde{a}_k \gamma_{thk}} \right\}$  and satisfying the conditions of  $a_1 > \tilde{a}_1 \gamma_{th1}, \dots, a_j > \tilde{a}_j \gamma_{thj}, \dots, a_k > \tilde{a}_k \gamma_{thk}$ . Note, that  $\varphi_k$  means to take out the biggest item from it, which can be obtained from (A1) with the help of some simple arithmetic operations. To calculate (A2), we should first provide the CDF of random  $X$  and the thermal noise power of  $Y$  caused by ARIS. Applying the coherent phase shifting and the Laguerre polynomial series [48] [Equation (2.76)], the CDF of  $X$  without order characteristics can be approximated as

$$F_X(x) \approx \frac{1}{\Gamma(\delta_k + 1)} \gamma \left( \delta_k + 1, \frac{\sqrt{x}}{\varepsilon_k} \right), \quad (\text{A3})$$

where  $\delta_k = \frac{L[\mathbb{E}(X_k)]^2}{\mathbb{D}(X_k)}$ ,  $\varepsilon_k = \frac{\mathbb{D}(X_k)}{\mathbb{E}(X_k)}$ ,  $\mathbb{E}(X_k) = \mathbb{E}(|h_{sr}^l h_{rk}^l|) = \frac{\pi}{4(\kappa+1)} [L_{\frac{1}{2}}(-\kappa)]^2$ ,  $\mathbb{D}(X_k) = \mathbb{D}(|h_{sr}^l h_{rk}^l|) = 1 - \frac{\pi^2}{16(\kappa+1)^2} [L_{\frac{1}{2}}(-\kappa)]^4$ ,  $L_{\frac{1}{2}}(x) = e^{\frac{x}{2}} [(1-x)I_0(-\frac{x}{2}) - xI_1(-\frac{x}{2})]$  represents the Laguerre polynomial.  $I_0(\cdot)$  and  $I_1(\cdot)$  denote the modified Bessel functions of the first

kind with orders *zero* and *one*, respectively. In addition,  $Y = |\mathbf{h}_{rk}^H \Lambda|^2 = \left| \sum_{l=1}^L h_{rk}^l e^{j\theta_l} \right|^2$ , since  $h_{rk}^l e^{j\theta_l}$  has the independent identical distribution for different  $l$ , we have the relationship of  $\mathbb{E} \left( \left| \sum_{l=1}^L h_{rk}^l e^{j\theta_l} \right|^2 \right) = \mathbb{D} \left( \left| \sum_{l=1}^L h_{rk}^l e^{j\theta_l} \right| \right) + \left[ \mathbb{E} \left( \left| \sum_{l=1}^L h_{rk}^l e^{j\theta_l} \right| \right) \right]^2$ . Based on statistical characteristics and simple operations,  $\mathbb{E} \left( |\mathbf{h}_{rk}^H \Lambda|^2 \right) = L \left( \frac{L\kappa+1}{\kappa+1} \right)$  can be obtained directly. Finally, substituting (A3) and thermal noise power  $\mathbb{E} \left( |\mathbf{h}_{rk}^H \Lambda|^2 \right)$  into (A2), and further applying the order statistical characteristics [16,49], we can obtain (7). The proof is completed.  $\square$

## References

1. ElMossallamy, M.A.; Zhang, H.; Song, L.; Seddik, K.G.; Han, Z.; Li, G.Y. Reconfigurable intelligent surfaces for wireless communications: Principles, challenges, and opportunities. *IEEE Trans. Cogn. Commun. Netw.* **2020**, *6*, 990–1002. [\[CrossRef\]](#)
2. Liu, Y.; Liu, X.; Mu, X.; Hou, T.; Xu, J.; Renzo, M.D.; Al-Dhahir, N. Reconfigurable intelligent surfaces: Principles and opportunities. *IEEE Commun. Surv. Tutor.* **2021**, *23*, 1546–1577. [\[CrossRef\]](#)
3. Wu, Q.; Zhang, S.; Zheng, B.; You, C.; Zhang, R. Intelligent reflecting surface-aided wireless communications: A tutorial. *IEEE Trans. Commun.* **2021**, *69*, 3313–3351. [\[CrossRef\]](#)
4. Basar, E.; Poor, H.V. Present and future of reconfigurable intelligent surface-empowered communications. *IEEE Signal Process. Lett.* **2021**, *38*, 146–152. [\[CrossRef\]](#)
5. Wang, X.; Han, J.; Tian, S.; Xia, D.; Li, L.; Cui, T. Amplification and manipulation of nonlinear electromagnetic waves and enhanced nonreciprocity using transmissive space-time-coding metasurface. *Adv. Sci.* **2022**, *9*, 2105960. [\[CrossRef\]](#) [\[PubMed\]](#)
6. Liu, Y.; Yi, W.; Ding, Z.; Liu, X.; Dobre, O.A.; Al-Dhahir, N. Developing NOMA to next generation multiple access: Future vision and research opportunities. *IEEE Wirel. Commun.* **2022**, *29*, 120–127. [\[CrossRef\]](#)
7. Ding, Z.; Liu, Y.; Choi, J.; Sun, Q.; Elkashlan, M.; Li, C.L.; Poor, H.V. Application of non-orthogonal multiple access in LTE and 5G networks. *IEEE Commun. Mag.* **2017**, *55*, 185–191. [\[CrossRef\]](#)
8. Li, X.; Li, J.; Liu, Y.; Ding, Z.; Nallanathan, A. Residual transceiver hardware impairments on cooperative NOMA networks. *IEEE Trans. Wirel. Commun.* **2020**, *19*, 680–695. [\[CrossRef\]](#)
9. Rabie, K.; Makarfi, A.U.; Kharel, R.; Badarneh, O.S.; Adebisi, B.; Li, X.; Ding, Z. On the performance of non-orthogonal multiple access over composite fading channels. *arXiv* **2021**, arXiv:2004.07860.
10. Wan, D.; Huang, R.; Wen, M.; Chen, G.; Ji, F.; Li, J. A simple multicarrier transmission technique combining transmit diversity and data multiplexing for non-orthogonal multiple access. *IEEE Trans. Veh. Technol.* **2021**, *70*, 7216–7220. [\[CrossRef\]](#)
11. Ding, Z. NOMA beamforming in SDMA networks: Riding on existing beams or forming new ones? *IEEE Commun. Lett.* **2022**, *26*, 868–871. [\[CrossRef\]](#)
12. Pei, X.; Chen, Y.; Wen, M.; Yu, H.; Panayirci, E.; Poor, H.V. Next-generation multiple access based on NOMA with power level modulation. *IEEE J. Sel. Areas Commun.* **2022**, *40*, 1072–1083. [\[CrossRef\]](#)
13. Xu, X.; Liu, Y.; Mu, X.; Chen, Q.; Ding, Z. Cluster-free NOMA communications towards next generation multiple access. *IEEE Trans. Commun.* **2023**, *71*, 2184–2200. [\[CrossRef\]](#)
14. Ding, Z.; Poor, H.V. A simple design of IRS-NOMA transmission. *IEEE Commun. Lett.* **2020**, *24*, 1119–1123. [\[CrossRef\]](#)
15. Zheng, B.; Wu, Q.; Zhang, R. Intelligent reflecting surface-assisted multiple access with user pairing: NOMA or OMA? *IEEE Commun. Lett.* **2020**, *24*, 753–757. [\[CrossRef\]](#)
16. Yue, X.; Liu, Y. Performance analysis of intelligent reflecting surface assisted NOMA networks. *IEEE Trans. Wirel. Commun.* **2022**, *21*, 2623–2636. [\[CrossRef\]](#)
17. Elhattab, M.; Arfaoui, M.A.; Assi, C.; Ghrayeb, A. Reconfigurable intelligent surface enabled full-duplex/half-duplex cooperative non-orthogonal multiple access. *IEEE Trans. Wirel. Commun.* **2022**, *21*, 3349–3364. [\[CrossRef\]](#)
18. Ding, Z.; Lv, L.; Fang, F.; Dobre, O.A.; Karagiannidis, G.K.; Al-Dhahir, N.; Schober, R.; Poor, H.V. A state-of-the-art survey on reconfigurable intelligent surface-assisted non-orthogonal multiple access networks. *Proc. IEEE* **2022**, *110*, 1358–1379. [\[CrossRef\]](#)
19. Khaleel, A.; Basar, E. A novel NOMA solution with RIS partitioning. *IEEE J. Sel. Areas Commun.* **2022**, *16*, 70–81. [\[CrossRef\]](#)
20. de Souza Junior, W.; Abrao, T. RIS-aided cooperative FD-SWIPT-NOMA outage performance in nakagami- $m$  channels. *arXiv* **2022**, arXiv:2204.01900.
21. Li, X.; Xie, Z.; Huang, G.; Zhang, J.; Zeng, M.; Chu, Z. Sum rate maximization for RIS-aided NOMA with direct links. *IEEE Netw. Lett.* **2022**, *4*, 55–58. [\[CrossRef\]](#)
22. Wang, H.; Shi, Z.; Fu, Y.; Fu, S. On intelligent reflecting surface-assisted NOMA uplinks with imperfect SIC. *IEEE Wirel. Commun. Lett.* **2022**, *11*, 1518–1522. [\[CrossRef\]](#)
23. Pei, Y.; Yue, X.; Yi, W.; Liu, Y.; Li, X.; Ding, Z. Secrecy outage probability analysis for downlink RIS-NOMA networks with on-off control. *IEEE Trans. Veh. Technol.* **2023**, *72*, 11772–11786. [\[CrossRef\]](#)
24. Zhao, H.; Kong, Z.; Huang, H.; Shi, S.; Ni, Y.; Gui, G.; Gacanin, H.; Sari, H.; Adachi, F. Air reconfigurable intelligent surface enhanced multi-user noma system. *IEEE Internet Things J.* **2023**, *11*, 29–39. [\[CrossRef\]](#)
25. Selvan, K.T.; Janaswamy, R. Fraunhofer and fresnel distances: Unified derivation for aperture antennas. *IEEE Antennas Propag. Mag.* **2017**, *59*, 12–15. [\[CrossRef\]](#)

26. Long, R.; Liang, Y.-C.; Pei, Y.; Larsson, E.G. Active reconfigurable intelligent surface-aided wireless communications. *IEEE Trans. Commun.* **2021**, *20*, 4962–4975. [[CrossRef](#)]
27. Khoshafa, M.H.; Ngatched, T.M.N.; Ahmed, M.H.; Ndjiongue, A.R. Active reconfigurable intelligent surfaces-aided wireless communication system. *IEEE Commun. Lett.* **2021**, *25*, 3699–3703. [[CrossRef](#)]
28. Zhang, Z.; Dai, L.; Chen, X.; Liu, C.; Yang, F.; Poor, H.V. Active RIS vs. passive RIS: Which will prevail in 6G? *IEEE Trans. Commun.* **2023**, *71*, 1707–1725. [[CrossRef](#)]
29. You, C.; Zhang, R. Wireless communication aided by intelligent reflecting surface: Active or passive? *IEEE Wirel. Commun. Lett.* **2021**, *10*, 2659–2663. [[CrossRef](#)]
30. Zhi, K.; Pan, C.; Ren, H.; Chai, K.K.; Elkashlan, M. Active RIS versus passive RIS: Which is superior with the same power budget? *IEEE Commun. Lett.* **2022**, *26*, 1150–1154. [[CrossRef](#)]
31. Liu, K.; Zhang, Z.; Dai, L.; Xu, S.; Yang, F. Active reconfigurable intelligent surface: Fully-connected or sub-connected? *IEEE Commun. Lett.* **2022**, *26*, 167–171. [[CrossRef](#)]
32. Zeng, P.; Qiao, D.; Wu, Q.; Wu, Y. Throughput maximization for active intelligent reflecting surface-aided wireless powered communications. *IEEE Wirel. Commun. Lett.* **2022**, *11*, 992–996. [[CrossRef](#)]
33. Nguyen, N.T.; Vu, Q.-D.; Lee, K.; Juntti, M. Hybrid relay-reflecting intelligent surface-assisted wireless communication. *IEEE Trans. Veh. Technol.* **2022**, *71*, 6228–6244. [[CrossRef](#)]
34. Kang, Z.; You, C.; Zhang, R. Active-passive IRS aided wireless communication: New hybrid architecture and elements allocation optimization. *IEEE Trans. Commun.* **2023**. [[CrossRef](#)]
35. Mohamed, R.; Emanuele, G.; Luca, V.; Stefano, B. Spatial diversity in radar detection via active reconfigurable intelligent surfaces. *IEEE Signal Process. Lett.* **2022**, *20*, 1242–1246.
36. Yang, X.; Wang, H.; Feng, Y. Sum rate maximization for active RIS-aided uplink multi-antenna NOMA systems. *IEEE Wirel. Commun. Lett.* **2023**, *12*, 1149–1153. [[CrossRef](#)]
37. Chen, G.; Wu, Q.; He, C.; Chen, W.; Tang, J.; Jin, S. Active IRS aided multiple access for energy-constrained IoT systems. *IEEE Trans. Wirel. Commun.* **2023**, *22*, 1677–1694. [[CrossRef](#)]
38. Shi, Z.; Lu, H.; Xie, X.; Yang, H.; Huang, C.; Cai, J.; Ding, Z. Active RIS-aided EH-NOMA networks: A deep reinforcement learning approach. *arXiv* **2023**, arXiv:2304.12184.
39. Luo, H.; Lv, L.; Wu, Q.; Ding, Z.; Al-Dhahir, N.; Chen, J. Beamforming design for active IOS aided NOMA networks. *IEEE Wirel. Commun. Lett.* **2023**, *12*, 282–286. [[CrossRef](#)]
40. Niu, H.; Lin, Z.; An, K.; Wang, J.; Zheng, G.; Al-Dhahir, N.; Wong, K.-K. Active RIS assisted rate-splitting multiple access network: Spectral and energy efficiency tradeoff. *IEEE J. Sel. Areas Commun.* **2023**, *41*, 1452–1467. [[CrossRef](#)]
41. Yue, X.; Song, M.; Ouyang, C.; Liu, Y.; Li, T.; Hou, T. Exploiting active RIS in NOMA networks with hardware impairments. *IEEE Trans. Veh. Technol.* **2024**, 1–15. [[CrossRef](#)]
42. Swindlehurst, A.L.; Zhou, G.; Liu, R.; Pan, C.; Li, M. Channel estimation with reconfigurable intelligent surfaces—A general framework. *Proc. IEEE* **2022**, *38*, 883–917. [[CrossRef](#)]
43. Zheng, B.; You, C.; Mei, W.; Zhang, R. A survey on channel estimation and practical passive beamforming design for intelligent reflecting surface aided wireless communications. *IEEE Commun. Surv. Tutor.* **2022**, *24*, 1035–1071. [[CrossRef](#)]
44. Ding, Z.; Yang, Z.; Fan, P.; Poor, H.V. On the performance of non-orthogonal multiple access in 5G systems with randomly deployed users. *IEEE Signal Process. Lett.* **2014**, *21*, 1501–1505. [[CrossRef](#)]
45. Hildebrand, E. *Introduction to Numerical Analysis*; Dover: New York, NY, USA, 1987.
46. Gradshteyn, I.S.; Ryzhik, I.M. *Table of Integrals, Series and Products*, 6th ed.; Academic Press: New York, NY, USA, 2000.
47. Zheng, L.; Tse, D. Diversity and multiplexing: A fundamental tradeoff in multiple-antenna channels. *IEEE Trans. Inf. Theory* **2003**, *49*, 1073–1096. [[CrossRef](#)]
48. Primak, V.K.S.; Lyandres, V. *Stochastic Methods and Their Applications to Communications: Stochastic Differential Equations Approach*; Wiley: West Sussex, UK, 2004.
49. David, H.A.; Nagaraja, H.N. *Order Statistics*, 3rd ed.; John Wiley: New York, NY, USA, 2003.

**Disclaimer/Publisher’s Note:** The statements, opinions and data contained in all publications are solely those of the individual author(s) and contributor(s) and not of MDPI and/or the editor(s). MDPI and/or the editor(s) disclaim responsibility for any injury to people or property resulting from any ideas, methods, instructions or products referred to in the content.